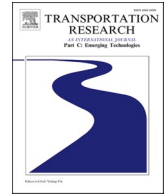




ELSEVIER

Contents lists available at [ScienceDirect](https://www.sciencedirect.com)

# Transportation Research Part C

journal homepage: [www.elsevier.com/locate/trc](http://www.elsevier.com/locate/trc)


## Collision probability between intruding drone and commercial aircraft in airport restricted area based on collision-course trajectory planning

Na Zhang<sup>b</sup>, Hu Liu<sup>b</sup>, Bing Feng Ng<sup>a</sup>, Kin Huat Low<sup>a,\*</sup><sup>a</sup> School of Mechanical and Aerospace Engineering, Nanyang Technological University, Singapore 639798, Singapore<sup>b</sup> Air Traffic Management Research Institute (ATMRI), Nanyang Technological University, Singapore 637460, Singapore

### ARTICLE INFO

#### Keywords:

Trajectory planning  
Stochastic kinematic model  
Relative position prediction  
Collision probability

### ABSTRACT

With the significant improvements in drone technology and the popularization of drones among their hobbyists, the incidents of drones intruding airports have resulted in a large number of flight delays and temporary closure of runways. To minimize the interference of drones on normal operations in the airports, a collision probability evaluation scheme based on collision-course trajectories modeling is proposed in this work. Firstly, a trajectory planning model of drones intruding restricted airspace is derived based on a given trajectory of the commercial aircraft (CA) and the collision-course scenario of the drone. Subsequently, according to the trajectories of the drone and CA, a probabilistic model based on the stochastic kinematic model is developed to implement the collision risk evaluation. The proposed method is first comparatively demonstrated with the Monte-Carlo (MC) simulation and several special cases with known drone's trajectories. Subsequently, the cases covering different drone's initial positions, positions updates, and different collision zones are simulated and analyzed using the proposed collision-course based model. The simulation results show that the established model can be employed to evaluate the collision probability, even if the trajectory information of the intruding drone is limited.

### 1. Introduction

The easy-to-operate feature and affordable price of drones lower the entry barrier for many users in various applications. However, such a trend for drones, as it grows, has posed a huge threat to the safe and efficient operation of airports around the world (Barlow et al., 2019; Schaufele et al., 2017; Schlag, 2012; Arblaster, 2018; Liu et al., 2020). Drones were frequently reported to intrude into the restricted airspace of the airport without any reporting in advance, which disrupts the normal take-off and approach of the commercial aircraft (CA). To avoid drones that broke into airports abruptly and ensure the safe operation of CA in terminal areas, measures have been taken in relevant airports, such as the installation of anti-drone systems and closure of runways (Deulgaonkar, 2017; Shi et al., 2018; Michalski and Michalska, 2017; Sturdivant and Chong, 2017). Besides, the approaches that are currently adopted by most airports is that once a drone is found near the airport, the runways will be temporarily closed for several hours and even longer until the danger is completely eliminated. Behind the implementation of this measure is that flights that take off at the original time have to postpone the flight plans, while flights that are ready to land at the destination airports have to be diverted to other airports, or even

\* Corresponding author.

E-mail address: [mkhlow@ntu.edu.sg](mailto:mkhlow@ntu.edu.sg) (K.H. Low).

<https://doi.org/10.1016/j.trc.2020.102736>

Received 29 December 2019; Received in revised form 20 May 2020; Accepted 23 July 2020  
0968-090X/© 2020 Elsevier Ltd. All rights reserved.

return to their departure airports. This guarantee measure for flight safety takes a toll on airports and passengers. Such flight delays and diversions not only cause the financial losses of the airports, but also make the passengers lose confidence in the airports due to the disruptive to their expected travel plans (Balakrishnan, 2016; Du et al., 2018). As the potential collision risks caused by the intruding drone activities to CA in terminal areas might lead to immeasurable disasters, aviation sectors and related research groups have emphasized on the importance of studying risk evaluation and collision prevention between the intruding drone and CA.

There is extensive work devoted to the risk assessment of collision between air vehicles, i.e. CA-to-CA. The mainstream idea is to predict the flight path of the aerial vehicles (including drones and commercial aircraft), and then to evaluate the collision probability on the assumption that the position error yields to the Gaussian distribution (Paielli and Erzberger, 1997; Sun et al., 2019b; Peng et al., 2020). The evaluation results can next be used to design the collision avoidance or conflict resolution actions. Following similar thoughts, flight trajectories have commonly been handled by the Kalman filter (Dogan and Zengin, 2006; Stubberud and Kramer, 2007; Teixeira et al., 2011). By employing the prior data in the probabilistic threat exposure map, the Kalman filter-based method was presented to estimate the coefficients of the dynamic-target pursuit models (Dogan and Zengin, 2006). By combining the augmented Kalman filter and neural network algorithm, the neural Kalman filter was developed to establish a target-tracking system to improve the position tracking of the target (Stubberud and Kramer, 2007). The extended Kalman filter is another established variant of the Kalman filter in trajectory prediction, which is often introduced to do position estimation of a moving object (Luo et al., 2013; Prevost et al., 2007; Driessen et al., 2018).

The disturbance of uncertainty is an important factor to be considered in flight path prediction and collision risk evaluation of CA-to-CA. The Partially Observable Markov Decision Process (POMDP) is taken as the preferable method for dealing with uncertain states, especially for the stochastic flight environment (Chryssanthacopoulos and Kochenderfer, 2011; Qiming et al., 2019; Bai et al., 2012; Sun et al., 2019a). To reveal the state uncertainty due to the sensor limitations and external disturbance in collision avoidance, a dynamic programming based POMDP framework was presented to tackle the drawback of the point estimation method (Chryssanthacopoulos and Kochenderfer, 2011). MC-based methods are also widely used to simulate the future flight path, evaluate conflict probability and verify conflict detection (Glover and Lygeros, 2004; Prandini and Watkins, 2005; Maracich, 2006).

The methods aforementioned are applicable to the collision risk assessment of CA-to-CA and cooperative drone-to-CA cases. To be specific, the missions and flight trajectories are known for the cooperative drones and CA due to the registered information, flight mission report in advance and sound air-to-air and air-to-ground devices, such as Traffic Alert and Collision Avoidance System (TCAS), Automatic Dependent Surveillance-Broadcast (ADS-B), and radar. TCAS installed on every CA, known as “the last line of defense against collisions”, is widely applied to monitor, track and predict the movement trend of the target aircraft within its available scope. The collision risk between one CA and its target CA is comprehensively evaluated by combining the motion direction, flight speed, flight attitude and other information of that CA and the predicted position information of its target CA in TCAS (Tang et al., 2018; Netjasov et al., 2019). According to the horizontal and vertical distances between one CA and its approaching target CA at the closest point of approach, the TCAS can predict and judge whether the CA collides with its target CA based on the consideration that only when the horizontal and vertical distances are less than the safety threshold at the same time can the collision between two CA be determined by anti-collision logic of TCAS (Romli et al., 2008; Tang, 2017; Radanovic et al., 2018). ADS-B system realizes traffic surveillance and information transmission using air-to-ground and air-to-air data link based on the global positioning system. The aircraft equipped with ADS-B can broadcast precise positions and other data (such as speed, altitude and whether the aircraft turns, climbs or descends, etc.) through the data link (Kacem et al., 2017; Riahi Manesh and Kaabouch, 2017; Ali, 2016). ADS-B receiver provides accurate and real-time conflict information in air and ground when combined with the air traffic control systems and other aircraft’s airborne ADS-B. This enables flight information sharing, especially trajectory information, and effectively improve the cooperation ability between air vehicles, enhance the performance of TCAS. During the process of aircraft operation, the ADS-B system will not only keep the minimum safety interval but also avoid and resolve the conflict of air-to-air coordination. This capability makes the responsibility of maintaining flight safety interval more transferred to the air, which is the indispensable technical basis for realizing “free flight”.

As for the collision risk of intruding drone-to-CA, related studies and evaluation methods are limited. This could be because of unknown or unavailable airborne communication systems of the drones, which brings great difficulties in tracking their trajectories. Generally, intruding drones are controlled by their operators and their missions will not be reported to authorities of airports, so their trajectories are unknown. On the other hand, those existing techniques used in airports to guarantee CA’s safe operation cannot be directly adopted to detect and evaluate the collision risk of intruding drones in low-altitude due to various reasons. Firstly, TCAS only works when the approaching target holds transponder and has the intention of coordination to resolve the collision. For intruding drones, their intentions and whether they have transponders are often unknown. Moreover, the resolution advisory (RA) function of TCAS fails to provide part of the prompt information when aircraft fly in the low-altitude (Munoz et al., 2013; Tang et al., 2016). For instance, when the take-off altitude is below 1200ft or the approach altitude is below 1000ft, RA has no descent prompt. Even if an intruding drone has a transponder and is willing to coordinate with a CA to remove the collision risk, the TCAS might not fully play its collision avoidance role in low-altitude airspace. Secondly, although air traffic controllers have achieved the low-altitude airspace surveillance by using low-altitude primary surveillance radar and navigable ADS-B transceiver (Lascara et al., 2013; Roudet et al., 2016; Zhang et al., 2018), ADS-B can only accomplish the intercommunication of position information when both air vehicles are equipped with information transmission and response devices. The high cost and heavyweight of commercially-available ADS-B affect the popularity of the most cooperative drones equipped with the device, not to mention those unknown intruding drones. Besides, many drones are made of various materials, it is therefore difficult to be found by low-altitude primary surveillance radar because of the small reflection echo. Also, some intruding drones are not high-speed threat targets, similar to birds, which is not easily detected by radar systems.

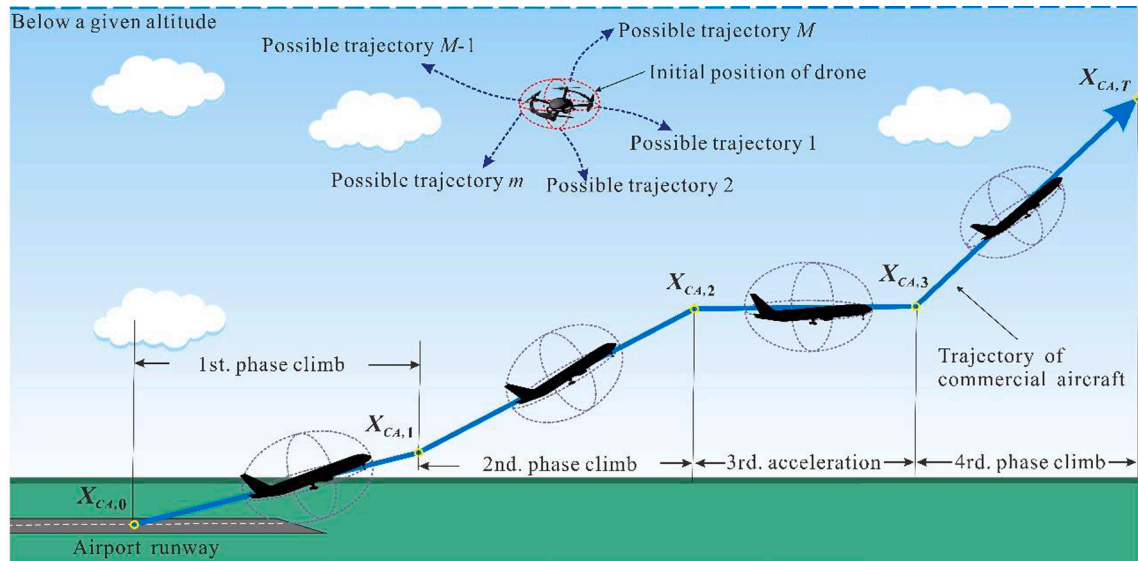


Fig. 1. A scenario where a drone is above an airport runway.

The research works to date mainly solve the problems of collision avoidance for CA-to-CA and cooperative drone-to-CA, whereas there are a few works on the collision probability of intruding drones-to-CA. In recent studies, a collision risk model was introduced to assess the probability between general aviation and unmanned aircraft (La Cour-Harbo and Schjøler, 2019). The model considered the physical parameters and the numbers of aerial vehicles, which discussed the precision of the predicted results. From this work, some ideas can be extracted and applied to civil aviation to evaluate collision probability between the drone and CA, but the study covered only general aviation and civil aviation. Based on the probabilistic conflict map, the 3D MC simulation models were developed to evaluate the collision risk of unmanned aerial systems and aircraft in restricted airspace (Wang et al., 2019a, 2019b, 2020). The works predicted the motion path and collision risk based on the performance of the drone on the assumption that the intention of the drone operator in known scenarios and also the drone's position in one of the scenarios could be reported by ADS-B. Consequently, the practical application of the model is limited. Furthermore, the path prediction in ref. (Wang et al., 2019a) does not consider the interference of external and internal environment factors to the drone and CA in the airspace. Also, the reliability of the MC simulation results needs to be further verified due to limited iterations (up to 2000 iterations only).

In view of the undesired situation that the airport runways are forced to suspend by intruding drones and the lack of improved surveillance and management technologies that airports can currently carry out for those drones, it is essential to develop a method to assist in realizing a safer and more efficient airspace management system. In this paper, a probabilistic model between the intruding drone and CA is developed based on the collision-course trajectory planning to implement collision probability evaluation. The main contribution of the proposed model includes: (1) A collision-course based trajectory model is developed to solve the problem of how to plan the flight trajectories of intruding drones in terms of the limited information; (2) A relative position prediction model is proposed to evaluate collision probability between the drone and CA by considering deviation caused by uncertainties.

The remaining of this paper is arranged as follows: Section 2 briefly analyzes the problem related to the trajectory prediction of the intruding drones will be briefly analyzed in Section 2, followed by the introduction of the collision-course based trajectory planning method. Section 3 elaborates details of the collision probability evaluation model, while simulation results are given and discussed in Section 4. Section 5 concludes the findings of the proposed collision probability evaluation method.

## 2. Trajectory planning

### 2.1. Problem analysis

Considering a scenario in which a CA is going to take off from or approaching an airport, an intruding drone suddenly appears near the airport. To ensure the safety of the CA, the airport or the pilot has to take action to such an incident. The immediate question is what actions should be taken. Any action should depend on the intention of the intruding drone. However, the operation of the intruding drone is controlled by its operator and no one knows the intention of the intruding drone in the actual situation. As shown in Fig. 1, it is assumed that the drone intrudes into the runway with different possible trajectories (1, 2, ...,  $m$ , ...,  $M-1$ ,  $M$ ), which poses a threat to the CA within the no-fly zone of the drone. The intention of the operator is unknown and the drone could fly in any directions. No device installed on the drone can be used by the control center of the airport to carry out collision avoidance command, only the initial position can be obtained by vision-based ways. In this case, to enable one to make reasonable measures by assessing the collision risk of the drone to a taking-off or approaching CA, a collision-course based trajectory scheme of the drone is presented.

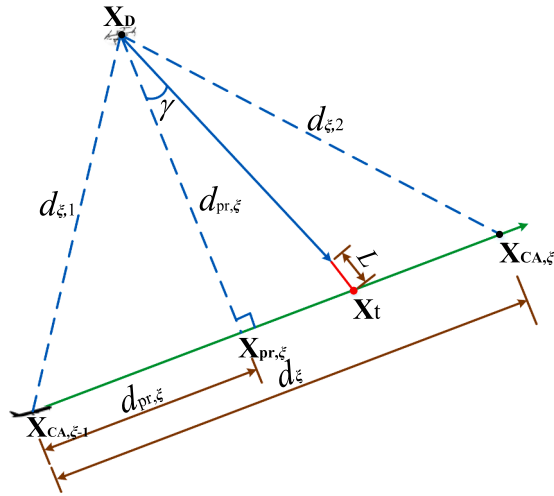


Fig. 2. Collision-course based trajectory planning of the intruding drone in the CA's operation phase  $\xi$ .

### 2.2. Collision-course based trajectory planning

For the modeling presented in this section, the collision time and angle between the intruding drone and CA in low-altitude airspace are determined based on the limited known information of the CA to further determine the velocity of the intruding drone. Given the speed of CA ( $V_{CA}$ ), which can be obtained from the flight plan or ADS-B and the initial position ( $X_D$ ) of the intruding drone. It is assumed that the drone intentionally intrudes into the airport area and tends to collide with the CA that is going to take off. The collision-course based trajectory planning of the drone is applied in this case. Specifically, the collision-course implies that the intruding drone deliberately takes the CA as the target and keeping the course unchanged with its best effort during the intruding process. We then define the initial position of CA,  $X_{CA,0}$ , as that the nosewheel of the CA leaves the ground at the end of taxiing, and the modeling geographical area is no-fly zones, in general, 5 km or 7 km away from the head center of the runway, and specific data depend on the relevant airport's regulations. In the proposed model, we take the CA as the reference object and set  $X_{CA,0}$  as  $(0, 0, 0)$ . Correspondingly, the initial position of the drone is the counterpart to the initial position of the CA, which can be obtained through airport runway surveillance technology, such as radio frequency based techniques. The drone's position can then be transformed into the coordinate system of the CA. The time the CA spent to escape from this area is then denoted as  $T$ , and the last position of CA then be denoted as  $X_{CA,T}$ . The speed of the intruding drone is set as  $V_D$  based on the collision-course rule.

Within the no-fly zone with 5 km around the runway, the CA experiences several phases, denoted as  $\xi$  ( $\xi = 1, 2, 3, \dots$ ), to take off and climb. In our current work, the total number of  $\xi$  is taken as 4, as shown in Fig. 1. Taking one of the flight phases  $\xi$  as an example to illustrate the collision-course based modeling, as shown in Fig. 2. In this low-altitude airspace, to ensure the safe operation, CA cannot change the course arbitrarily within such a short duration from  $X_{CA,\xi-1}$  to  $X_{CA,\xi}$ . Therefore the geometrical length of its operation can be approximately regarded as the straight line. For the whole modeling area, the trajectory of the CA consists of different takeoff phases from the initial position  $X_{CA,0}$  to the position  $X_{CA,T}$ , where the CA flies out of the no-fly zone. Furthermore, within the no-fly zone, by considering the takeoff speed of CA, 200–300 km/h, the duration of CA will take no more than 150 s. During such a short operation period, CA climb with a varying acceleration (in the estimation of engineering practice, the takeoff acceleration can be assumed constant). Based on these assumptions, an integral model of collision-course is established.

When the position of intruding drone  $X_D$  is detected and by assuming that the projection of  $X_D$  on each CA's phase is  $X_{pr,\xi}$ , if there exists a  $t$  ( $t \in [0, T]$ ) such that collision occurs in the phase  $\xi$ , we have

$$\int_{t_{\xi-1}}^t V_{CA,\xi} dt = d_{pr,\xi} + (V_D t + L) \sin \gamma \tag{1}$$

where  $t_{\xi-1}$  is the initial time of the phase  $\xi$  (also the end time of the phase  $\xi - 1$ ),  $d_{pr,\xi}$  is the distance between  $X_{CA,\xi-1}$  and  $X_{pr,\xi}$ , and  $L$  ( $L \in [0, r]$ ) is the collision tolerance considering the geometrical dimension of the two aerial vehicles. The position of CA at the time  $t$  can be defined as the collision point  $X_t$  and  $\gamma$  is the collision angle that determines the velocity vector of the drone. Here,  $\gamma \in \left[ 0, \cos \frac{d_{\xi,1}^2 + d_{\xi,2}^2 - d_{\xi}^2}{2d_{\xi,1} d_{\xi,2}} \right)$ ,  $d_{\xi,1}$ ,  $d_{\xi,2}$  and  $d_{\xi}$  are the distances between  $X_{CA,\xi-1}$  and  $X_D$ , between  $X_D$  and  $X_{CA,\xi}$ , and between  $X_{CA,\xi-1}$  and  $X_{CA,\xi}$ , respectively.

Next, the irregular speeds of CA in phase  $\xi$  are divided into different time intervals  $[t_{\xi,u}, t_{\xi,u+1}) \in t_{\xi}$ . Every interval covers the same speed value so as to facilitate the computation of the following equation:

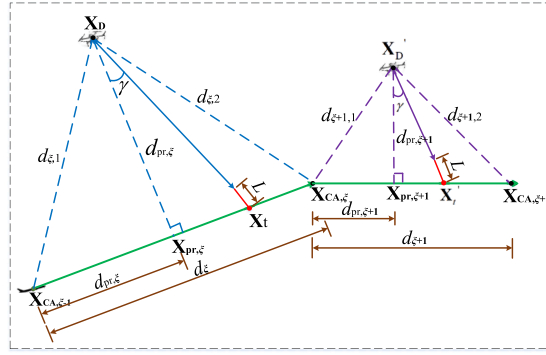


Fig. 3. Model update under the collision-course trajectory planning of two adjacent phases.

$$\sum_{u=1}^U V_{CA,u} \Delta t_{\xi,u} + \left( t - \sum_{u=1}^U \Delta t_{\xi,u} - t_{\xi-1} \right) V_{CA,U+1} = d_{pr,\xi} + (V_D t + L) \sin \gamma \quad (2)$$

where  $U$  is the number of changes of CA's speeds within collision time  $t$ , and  $\Delta t_{\xi,u} = T_{\xi,u+1} - T_{\xi,u}$ . Here, as the size of collision tolerance  $L$  depends on the radius of the minimum collision zone, then when  $L \in [0, r_{min}]$ , let the range of  $\gamma$  be  $\gamma \in [\gamma_{rmin}, \gamma_0]$ , in which  $\gamma_0$  and  $\gamma_{rmin}$  are the values when  $L = 0$  and  $L = r_{min}$ , respectively. For each collision angle  $\gamma$  in  $[\gamma_{rmin}, \gamma_0]$ , the corresponding collision-course based velocity of the drone can be determined.

It is worth mentioning that the collision-course based method reflects the average level of collision probability within the range of collision angle  $[\gamma_{rmin}, \gamma_0]$  due to the collision tolerance. In terms of the safety requirements of the CA, it is the most conservative trajectory planning method to evaluate collision probability. In other words, if the drone flies according to the trajectory obtained by the collision-course based model, the collision probability of the drone hitting the CA is the maximum collision probability within its performance range. On the other hand, if the actual flight trajectory of the drone is not the planned collision-course based trajectory, the probability of the drone flying along any other trajectory and colliding with the CA is then less than that of the drone flying according to the planned trajectory. Note that the collision-course based model can be implemented before the CA carries out the original flight plan to serve as the support information to help in deciding the action-to-be of the CA as soon as the airport detects an intruding drone.

Besides, updating the model in time helps to obtain more effective probability estimation information. The proposed trajectory planning model can be updated as long as the new position of the drone is reported, as illustrated in Fig. 3 where the collision occurred in  $X'_t$  with the drone's new position  $X'_D$ . With the update, the probabilistic results can be timely captured.

### 3. Collision probability evaluation

Considering that if there is not any interference in the low-altitude airspace, according to the planned trajectories of the intruding drone and CA, whether the drone collides with the CA or not is obvious based on the collision time and angle, as well as the velocity of the intruding drone presented in Section 2. However, this can be seen as an ideal scenario. In actual flight situations, the trajectory of aerial vehicles can be disturbed by various uncertainties. It will then places aerial vehicles into a random environment, and inevitably lead to the position prediction error of the flight trajectory (Chryssanthacopoulos and Kochenderfer, 2011; Sun et al., 2019a; Matsuno et al., 2015). By taking uncertainties into account, a relative position prediction model based on velocity and random noises is then introduced in this section to predict the collision probability of the intruding drone and CA.

#### 3.1. Position prediction of the drone and CA

Let the position and velocity vectors of the intruding drone and CA at the time  $t$  ( $t \in T$ ) be  $\mathbf{X}_D(t) \in \mathbb{R}^3$  and  $\mathbf{X}_{CA}(t) \in \mathbb{R}^3$ ,  $\mathbf{V}_D(t) \in \mathbb{R}^3$  and  $\mathbf{V}_{CA}(t) \in \mathbb{R}^3$ , respectively. Since aerial vehicles will inevitably be disturbed by various random process noises in the course of operation, the deviation in their planned trajectories can be modeled as noises. Therefore, the positions of the aerial vehicles can be determined by velocities along with disturbance, and the stochastic kinematic model of the drone and CA is constructed as

$$\begin{cases} d\mathbf{X}_D(t) = \mathbf{V}_D(t)dt + \mathbf{R}_D(\theta_D(t))\mathbf{C}_D(t)d\mathbf{B}_D(t) \\ d\mathbf{X}_{CA}(t) = \mathbf{V}_{CA}(t)dt + \mathbf{R}_{CA}(\theta_{CA}(t))\mathbf{C}_{CA}(t)d\mathbf{B}_{CA}(t) \end{cases} \quad (3)$$

where  $\mathbf{B}(t)$  is the standard 3D standard Brownian motion (BM) used to express random noise in conflict detection of aerial vehicles (Hu et al., 1999; Shi and Wu, 2012; Li and Cui, 2008). Note that  $\mathbf{R}(\theta(t))$  is the rotation matrices of drone and CA at time  $t$ , respectively. It is assumed that the influence of disturbance on the horizontal and vertical velocity of aerial vehicles is independent (Paielli and Erzberger, 1999),  $\mathbf{R}(\theta(t))$  can then be expressed as

$$\mathbf{R}(\theta(t)) = \begin{bmatrix} \cos(\theta(t)) & -\sin(\theta(t)) & 0 \\ \sin(\theta(t)) & \cos(\theta(t)) & 0 \\ 0 & 0 & 1 \end{bmatrix} \quad (4)$$

where  $\theta(t)$  represents the angle between the projection of the along-cross direction on the horizontal plane and the X-axis of the inertial coordinate system at the time  $t$  and  $\mathbf{C}(t)$  is the covariance matrix of position prediction error. Here,  $\mathbf{C}_{CA}(t)$  is denoted as

$$\mathbf{C}_{CA}(t) = \begin{bmatrix} \sigma_a^2(t) & 0 & 0 \\ 0 & \sigma_c^2(t) & 0 \\ 0 & 0 & \sigma_v^2(t) \end{bmatrix} \quad (5)$$

where  $\sigma_a^2(t)$ ,  $\sigma_c^2(t)$  and  $\sigma_v^2(t)$  are the variances of position prediction error in the along-track, cross-track and vertical directions, respectively and approximately obey Gaussian distribution (Prandini et al., 1999, 2000; Paielli and Erzberger, 1997), specifically,

$$\sigma_a^2(t) \sim g_a^2 t^2 \quad (6)$$

$$\sigma_c^2(t) \sim \min\{g_c^2 s^2(t), \sigma_{c,\max}^2\} \quad (7)$$

$$\sigma_v^2(t) \sim g_v^2 t^2 \quad (8)$$

where  $g_a^2$ ,  $g_c^2$  and  $g_v^2$  are the growth rates of variances of position prediction error for the along-track, cross-track and vertical directions, respectively,  $s(t)$  is the flight range of aerial vehicles and  $\sigma_{c,\max}^2$  is the maximum variance of the cross-track position prediction error. For the intruding drone, experimental variances are given thereafter. The relative position of the drone and CA can then be

$$d\Delta\mathbf{X}(t) = \Delta\mathbf{V}(t)dt + [\mathbf{R}_{CA}(\theta_{CA}(t))\mathbf{C}_{CA}(t)d\mathbf{B}_{CA}(t) - \mathbf{R}_D(\theta_D(t))\mathbf{C}_D(t)d\mathbf{B}_D(t)] \quad (9)$$

where  $\Delta\mathbf{X}(t) = \mathbf{X}_{CA}(t) - \mathbf{X}_D(t)$  and  $\Delta\mathbf{V}(t) = \mathbf{V}_{CA}(t) - \mathbf{V}_D(t)$ . It can be seen that the relative position of the drone and CA consists of two parts, one is the definite variable and another is a random variable.

### 3.2. Mean and covariance derivation of relative position error

The flight velocities change irregularly during the takeoff and climbing phases, therefore, when calculating the relative position of the drone and CA at time  $t$  by integrating Eq. (9), different upper and lower bounds of the integral can be divided according to the change of relative velocity. As the time interval of a certain flight state is included in an integral interval, the relative velocity can be regarded as a constant vector, and the corresponding rotation matrices  $\mathbf{R}_D(\theta_D(t))$  and  $\mathbf{R}_{CA}(\theta_{CA}(t))$  are also constant. Based on this, the general equations of the mean and variance of the relative position is deduced.

Let the velocity of an aerial vehicle be

$$\mathbf{V}(t) = \mathbf{V}_j \quad (10)$$

where  $\mathbf{V}_j$  is a constant vector,  $t \in [T_j, T_{j+1})$ ,  $T_j$  and  $T_{j+1}$  are the starting and ending points of a certain flight interval. For the drone and CA, the velocities  $\mathbf{V}_D(t)$  and  $\mathbf{V}_{CA}(t)$  are then constant vectors at each predicted position interval given by:

$$\begin{cases} \mathbf{V}_D(t) = \mathbf{V}_{D,i} & t \in [T_{D,i}, T_{D,i+1}), 0 \leq i \leq N_D \\ \mathbf{V}_{CA}(t) = \mathbf{V}_{CA,j} & t \in [T_{CA,j}, T_{CA,j+1}), 0 \leq j \leq N_{CA} \end{cases} \quad (11)$$

where  $T_{D,i}$  and  $T_{CA,j}$  are moments that the velocities of the drone and CA change,  $T_{D,0} = T_{CA,0} = 0$  and  $T_{D,N_D+1} = T_{CA,N_{CA}+1} = T$ ,  $N_D$  and  $N_{CA}$  are the change times of the  $\mathbf{V}_D(t)$  and  $\mathbf{V}_{CA}(t)$ , respectively, and  $T$  is the period that the CA operates in the terminal low-altitude airspace.

By combining the change time of the velocities of the drone and CA  $\{T_{D,i}\}, i = 0, 1, \dots, N_D + 1$  and  $\{T_{CA,j}\}, j = 0, 1, \dots, N_{CA} + 1$ , and by sorting them orderly to obtain  $\{T_k\}, k = 0, 1, \dots, N + 1$ , and  $N$  is the change times of the relative velocity, we have

$$\Delta\mathbf{V}(t) = \Delta\mathbf{V}_k \quad (12)$$

where  $t \in [T_k, T_{k+1}), 0 \leq k \leq N$  and  $\Delta\mathbf{V}_k$  is the relative velocity of the intruding drone and CA at the time interval  $[T_k, T_{k+1})$ .

When the relative velocity is a constant vector in each time interval, the corresponding predicted flight trajectory is a straight line, and the rotation matrices  $\mathbf{R}_D(\theta_D(t))$  and  $\mathbf{R}_{CA}(\theta_{CA}(t))$  are constant, which can be denoted as

$$\begin{cases} \mathbf{R}_D(\theta_D(t)) = \mathbf{R}_{D,k} \\ \mathbf{R}_{CA}(\theta_{CA}(t)) = \mathbf{R}_{CA,k} \end{cases} \quad t \in [T_k, T_{k+1}), 0 \leq k \leq N \quad (13)$$

According to the position prediction model, the predicted relative position of the drone and CA is a random variable related to the velocity and BM disturbance. Therefore, it is useful to analyze and derive the probability density function (PDF) of collision by integrating the relative predicted position according to different interval distributions of velocities.

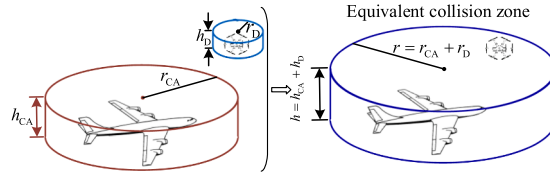


Fig. 4. Equivalent diagram of the minimum collision zone of the drone and CA.

Let  $t \in [T_0, T_1)$ , then the difference of relative position  $\Delta\mathbf{X}(t)$  at time  $t$  and  $\Delta\mathbf{X}(0)$  at  $t = 0$  can be obtained by the integral of Equation (9):

$$\Delta\mathbf{X}(t) - \Delta\mathbf{X}(0) = \Delta\mathbf{V}_0 t + \mathbf{R}_{CA,0} \mathbf{C}_{CA} [\mathbf{B}_{CA}(t) - \mathbf{B}_{CA}(0)] - \mathbf{R}_{D,0} \mathbf{C}_D [\mathbf{B}_D(t) - \mathbf{B}_D(0)] \quad (14)$$

where  $\Delta\mathbf{V}_0$ ,  $\mathbf{R}_{CA,0}$  and  $\mathbf{R}_{D,0}$  are constant values.

When  $t \in [T_k, T_{k+1})$ , the relative position  $\Delta\mathbf{X}(t)$  of the drone and CA obeys Gaussian distribution and by deducting Equation (14) (Hu et al., 1999), the corresponding mean  $\mu[\Delta\mathbf{X}(t)]$  and covariance  $\mathbf{C}[\Delta\mathbf{X}(t)]$  functions can be obtained as follows:

$$\mu[\Delta\mathbf{X}(T_k)] = \begin{cases} \mu[\Delta\mathbf{X}(T_0)] = \Delta\mathbf{X}_0, & k = 0 \\ \Delta\mathbf{X}_0 + \sum_{n=1}^k \Delta\mathbf{V}_{n-1} (T_n - T_{n-1}), & 0 < k \leq N \end{cases} \quad (15)$$

$$\mathbf{C}[\Delta\mathbf{X}(T_k)] = \begin{cases} \mathbf{C}_{CA,0} + \mathbf{C}_{D,0}, & k = 0 \\ \mathbf{C}_{CA,0} + \mathbf{C}_{D,0} + \sum_{n=1}^k (T_n - T_{n-1}) (\mathbf{R}_{CA,n-1} \mathbf{C}_{CA} \mathbf{R}_{CA,n-1}^T + \mathbf{R}_{D,n-1} \mathbf{C}_D \mathbf{R}_{D,n-1}^T), & 0 < k \leq N \end{cases} \quad (16)$$

$$\mu[\Delta\mathbf{X}(t)] = \mu[\Delta\mathbf{X}(T_k)] + \Delta\mathbf{V}_k (t - T_k) \quad (17)$$

$$\mathbf{C}[\Delta\mathbf{X}(t)] = \mathbf{C}[\Delta\mathbf{X}(T_k)] + (t - T_k) (\mathbf{R}_{CA,k} \mathbf{C}_{CA} \mathbf{R}_{CA,k}^T - \mathbf{R}_{D,k} \mathbf{C}_D \mathbf{R}_{D,k}^T) \quad (18)$$

Details of the derivation can be found in Appendix A.

### 3.3. Evaluation of collision probability

The collision probability of the drone and CA is that one intrudes the collision zone of another. Let the collision probability of each collision-course based trajectory of the drone and CA be  $P_m(t)$ , and then for all of the drone's trajectories  $M$  within the collision angle, the collision probability between the drone and CA can be defined as

$$P(t) = \frac{\sum_{m=1}^M P_m(t)}{M} \quad (19)$$

where  $M$  is the number of trajectories of the drone such that

$$\frac{\|^{M+1}P(t) - ^M P(t)\|}{^{M+1}P(t)} \leq \varepsilon \quad (20)$$

For each trajectory  $m$ , the PDF is  $p_m(\Delta\mathbf{X}_t) = p_m(\Delta x_t, \Delta y_t, \Delta z_t)$  at  $t \in [T_k, T_{k+1})$ . For clarity,  $p_m(\Delta\mathbf{X}_t)$  and  $p_m(\Delta x_t, \Delta y_t, \Delta z_t)$  are rewritten as  $p_m(\mathbf{X}_t)$  and  $p_m(x_t, y_t, z_t)$ , respectively, and the collision probability between the drone and CA can then be expressed as

$$P_m(t) = \iiint_{(x,y,z) \in \Omega} p_m(x_t, y_t, z_t) dx_t dy_t dz_t \quad (21)$$

where  $\Omega$  is the collision zone, and the minimum collision zone can be set as the equivalent zone composed of the geometric dimensions of the drone and CA, in which the equivalent size of collision radius and height are shown in Fig. 4. For collision risk evaluation, a safe separation distance can be determined by testing different sizes of the collision zone, i.e. incremental separation distance.

As the PDFs of the predicted relative position are not related in the horizontal and vertical directions each other (Paielli and Erzberger, 1999), we have

$$p_m(x_t, y_t, z_t) = p_{m,H}(x_t, y_t) p_{m,V}(z_t) \quad (22)$$

where  $p_{m,H}(x_t, y_t)$  and  $p_{m,V}(z_t)$  are respectively the PDFs of the horizontal and vertical relative positions. As the relative position yields to the Gaussian distribution,  $p_{m,H}(x_t, y_t)$  and  $p_{m,V}(z_t)$  can be written as the following equations, respectively,

$$p_{m, H}(x_t, y_t) = p_m(\mathbf{X}_t, t) = \frac{1}{2\pi\sqrt{|\mathbf{C}_{H, t}|}} \exp\left[-\frac{(\mathbf{X}_{H, t} - \mu_{H, t})^T \mathbf{C}_{H, t}^{-1} (\mathbf{X}_{H, t} - \mu_{H, t})}{2}\right] \quad (23)$$

$$p_{m, V}(z_t) = \frac{1}{\sqrt{2\pi}\sigma_{z_t}} \exp\left[-\frac{(z_t - \mu_{z_t})^2}{2\sigma_{z_t}^2}\right] \quad (24)$$

where  $\mathbf{X}_{H, t} = (x_t, y_t)^T$ ,  $T$  is the transpose symbol. The mean of the horizontal and vertical relative positions are  $\mu_{H, t} = (\mu_{x_t}, \mu_{y_t})^T$  and  $\mu_{z_t}$ , respectively. Next, the covariance matrix of the relative position  $\mathbf{C}(\mathbf{X}_t)$  can be rewritten as

$$\mathbf{C}(\mathbf{X}_t) = \begin{bmatrix} \mathbf{C}_{H, t} & 0 \\ 0 & \sigma_{z_t}^2 \end{bmatrix} \quad (25)$$

where  $\mathbf{C}_{H, t}$  is the covariance of the horizontal relative position and  $\sigma_{z_t}^2$  is the variance of the vertical relative position. The collision probability at time  $t$  is then written as

$$P_m(t) = P_{m, H}(t)P_{m, V}(t) \quad (26)$$

where

$$P_{m, H}(t) = \iint_{x_t^2 + y_t^2 \leq r^2} p_{m, H}(x_t, y_t) dx_t dy_t \quad (27)$$

$$P_{m, V}(t) = \int_{-\frac{h}{2} \leq z_t \leq \frac{h}{2}} p_{m, V}(z_t) dz_t = \int_{-\frac{h}{2}}^{\frac{h}{2}} \frac{1}{\sqrt{2\pi}\sigma_{z_t}} \exp\left[-\frac{(z_t - \mu_{z_t})^2}{2\sigma_{z_t}^2}\right] dz_t \quad (28)$$

in which  $r$  is the radius of the collision zone and  $h$  is the height of the collision zone.

With the derivation of Eq. (27) shown in Appendix B, the variances of relative position error  $\sigma_{x_t}^2$  and  $\sigma_{y_t}^2$  can be changed to uncorrelated in the axes  $x'$  and  $y'$ , we then have

$$P_{m, H}(t) = \iint_{x_t^2 + y_t^2 \leq r^2} p_{m, H}(x_t, y_t) dx_t dy_t = \iint_{(x'_t - a_t)^2 + (y'_t - b_t)^2 \leq r^2} p_{m, x'_t}(x'_t) p_{m, y'_t}(y'_t) dx'_t dy'_t \quad (29)$$

where  $p_{m, x'_t}(x'_t)$  and  $p_{m, y'_t}(y'_t)$  are the PDFs of the along-track and cross-track directions in the coordinate system  $x'_t O_{e_t} y'_t$  at time  $t$ , and both of them have a zero-mean but different variances  $\sigma_{x'_t}^2$  and  $\sigma_{y'_t}^2$  in their covariance matrix  $\mathbf{C}_{H, t}'$ . Assume that the two eigenvalues of the  $\mathbf{C}_{H, t}'$  are  $\lambda_1$  and  $\lambda_2$ , respectively, and  $\sigma_{x'_t}^2 = \max(\lambda_1, \lambda_2)$ ,  $\sigma_{y'_t}^2 = \min(\lambda_1, \lambda_2)$ . In details, we have

$$\mathbf{C}_{H, t}' = \mathbf{R} \mathbf{C}_{H, t} \mathbf{R}^T = \begin{pmatrix} \cos\varphi_{T_k} & -\sin\varphi_{T_k} \\ \sin\varphi_{T_k} & \cos\varphi_{T_k} \end{pmatrix} \mathbf{C}_{H, t} \begin{pmatrix} \cos\varphi_{T_k} & -\sin\varphi_{T_k} \\ \sin\varphi_{T_k} & \cos\varphi_{T_k} \end{pmatrix}^T \quad (30)$$

$$p_{m, x'_t}(x'_t) \sim N(0, \sigma_{x'_t}^2) \quad (31)$$

$$p_{m, y'_t}(y'_t) \sim N(0, \sigma_{y'_t}^2) \quad (32)$$

Then  $P_{m, H}(t)$  can be expressed as

$$P_{m, H}(t) = \iint_{(x'_t - a_t)^2 + (y'_t - b_t)^2 \leq r^2} p_{m, x'_t}(x'_t) p_{m, y'_t}(y'_t) dx'_t dy'_t = \int_{a_t - r}^{a_t + r} p_{m, x'_t}(x'_t) \left[ \int_{b_t - \sqrt{r^2 - (x'_t - a_t)^2}}^{b_t + \sqrt{r^2 - (x'_t - a_t)^2}} p_{m, y'_t}(y'_t) dy'_t \right] dx'_t \quad (33)$$

Let

$$f_m(x'_t) = p_{m, x'_t}(x'_t) \left[ \int_{b_t - \sqrt{r^2 - (x'_t - a_t)^2}}^{b_t + \sqrt{r^2 - (x'_t - a_t)^2}} p_{m, y'_t}(y'_t) dy'_t \right] \quad (34)$$

To solve this, the compound Simpson equation is used due to its high algebraic accuracy and good convergence. Let the integral limits be divided into  $2w$  equal parts, the integral step  $s$  can be

$$s = \frac{(a_t + r) - (a_t - r)}{2w} = \frac{r}{w} \quad (35)$$

**Table 1**  
Performance specs of DJI Mavic 2 and A320 (DJI Technology Co., 2019; Airbus, 2005).

	Variables	Values
Drone	Max speed	20 m/s (S-mode)
	Cruise speed	50 km/hr
	Max range	18 km
	Max ascend speed	5 m/s
	Max descent speed	3 m/s
	Dimensions (unfolded)	322 × 242 × 84 (mm; length × width × height)
CA	Max altitude	6000 m
	Take-off speed	74.6 m/s
	Dimensions	37.57 × 34.09 × 11.76 (m; length × wing span × height)

**Table 2**  
Takeoff and climb parameters of the CA (Zhu et al., 2016).

Phase $\xi$	Starting speed of $\xi$ (m/s)	Operation state	Duration (s)
1	61.03	Accelerating and climbing, $a = 0.15$ g	3.3
2	65.98	Constant climbing, $a = 0$	19.0
3	65.98	Horizontally accelerating, $a = 0.3$ g	10.0
4	95.98	Constant climbing, $a = 0$	37.6

**Table 3**  
MC comparative statistical results.

Methods	Indexes		Computational efficiency (s)
	$ e $	$ e _{max}$	
Proposed method	–	–	7.93
MC-5,000	8.3201E-04	1.8E-02	19.95
MC-10,000	2.03892E-04	3.48E-03	29.19
MC-50,000	4.60439E-05	1.17E-03	53.54
MC-100,000	8.23524E-07	4.52E-04	121.43
MC-200,000	3.17862E-09	7.82E-06	268.36

Note: the simulations are conducted on MATLAB R2019b software with Inter(R) Core(TM) i7-7500 CPU @ 2.70 GHz and 8.00 RAM with 4 cores.

and the collision probability between the drone with trajectory  $m$  and the CA is expressed as

$$\begin{aligned}
 P_{m, H}(t) &= \int_{a_t-r}^{a_t+r} f_m(x_t') dx_t' \\
 &\approx \frac{r}{3} \left[ f_m(a_t-r) + f_m(a_t+r) + \sum_{k=1}^{w-1} 2f_m(x_t, 2k') + \sum_{k=1}^{w-1} 4f_m(x_t, 2k-1') \right] \\
 &= \frac{r}{3w} \left[ f_m(a_t-r) + f_m(a_t+r) + \sum_{k=1}^{w-1} 2f_m(x_t, 2k') + \sum_{k=1}^{w-1} 4f_m(x_t, 2k-1') \right]
 \end{aligned} \tag{36}$$

Here, the truncation error is

$$E_{S_n}(f)_{max} = \frac{S^4}{180} (2r)_{max} |f^{(4)}(\zeta)| \tag{37}$$

where  $\zeta \in (a_t-r, a_t+r)$ .

#### 4. Simulation results

In this section, the simulations are conducted to validate the proposed method. The information of the drone is limited as it is sighted near the airport runway. In our study, it is assumed that the position of the intruding drone can be obtained roughly by vision-based mode, while the type of drone cannot be determined precisely because of its distance, etc. Therefore, the simulation parameters are assumed referring to the drone DJI Mavic 2 and commercial aircraft A320, as shown in Table 1. Especially, by considering that the velocity of CA is varying over time because of the constant change of lift and drag forces during takeoff, the changing velocities are set in total simulation time  $T = 70$  s and covered the four phases in the simulation. The specific parameters are listed in Table 2. The geometrical range is 5 km around the runway no-fly zone.

**Table 4**

Comparison of the computational efficiency of the proposed method and MC-50,000 with different computers.

Computer No.	Efficiency (s)	
	Proposed method	MC-50,000
Com. 1 (i7-7500 CPU @2.70 GHz and 8.00 RAM with 4 cores)	7.93	53.54
Com. 2 (i7-9700T CPU @4.30 GHz and 12 RAM with 16 cores)	4.65	38.57
Com. 3 (i9-9900K CPU @5.00 GHz and 16 RAM with 64 cores)	0.86	17.89

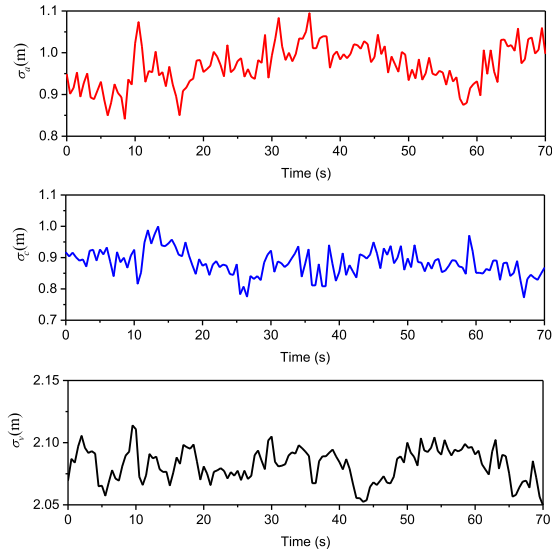


**Fig. 5.** The variances of the intruding drone in the along-track, cross-track, and vertical directions.

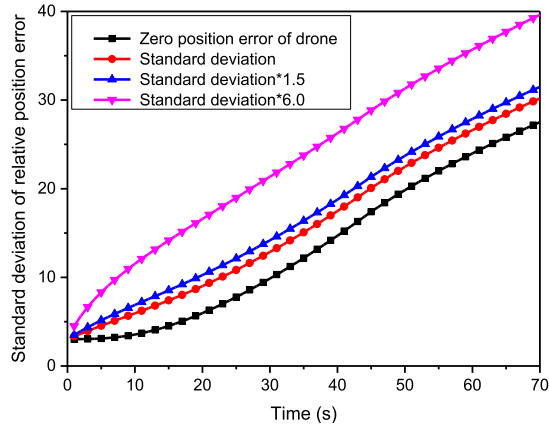


**Fig. 6.** Standard deviations of relative position error under different standard deviations of the intruding drone.

**4.1. Comparative validation with MC simulation and different deviations**

To demonstrate the computational performance of the proposed method, MC simulations covering 5,000, 10,000, 50,000, 100,000 and 200,000 iterations are utilized here and the comparative results are shown in Table 3. For clarity, mean absolute error  $|\bar{e}|$ , maximum absolute error  $|e_{max}|$  and computing efficiency are introduced to statistically compare the MC results given in Table 3, in which  $|\bar{e}| = avg(|P - P_{MC}|)$  and  $|e_{max}| = max(|P - P_{MC}|)$ . It can be seen from Table 3 that the  $|\bar{e}|$  and the  $|e_{max}|$  of the proposed method and MC simulation results are gradually reduced with the increase of the number of iterations. Especially when MC iterations reached 50,000, the results of the proposed algorithm and MC simulation fit each other very well. The maximum absolute error and mean absolute error are only 1.17E-03 and 4.60439E-05, respectively, which meets the accuracy requirements of collision probability well

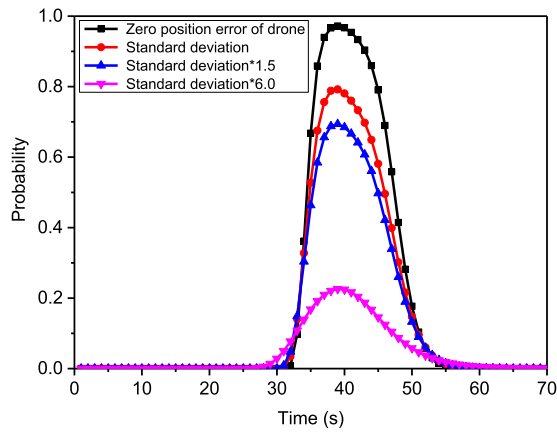
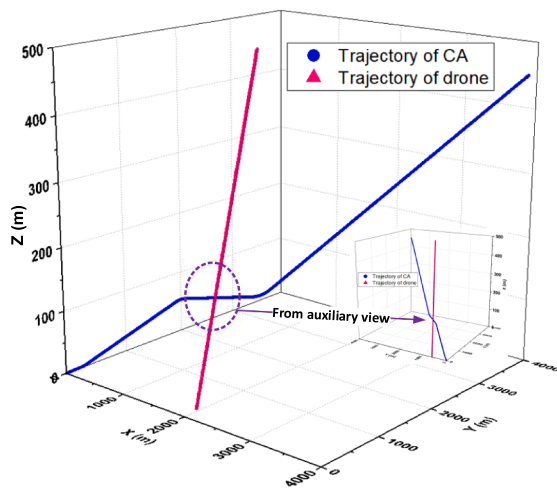
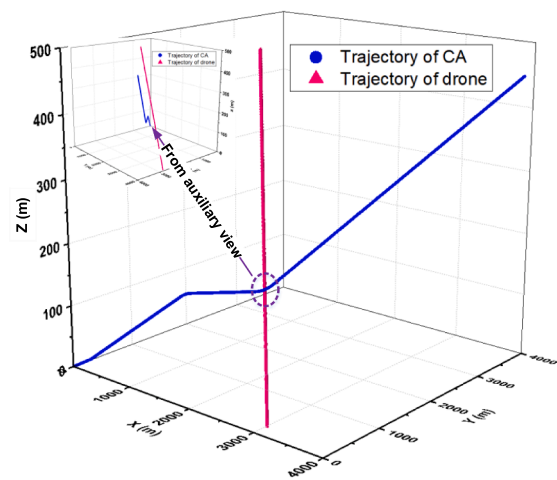


Fig. 7. The collision probability of different standard deviations of intruding drone to CA.



(a)



(b)

Fig. 8. Trajectories of the drone and CA with (a) collision and (b) non-collision.

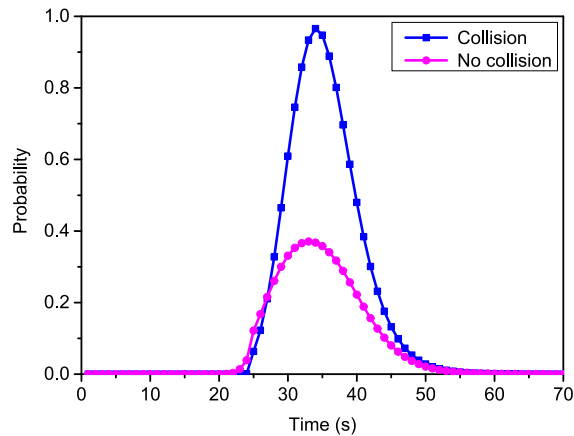


Fig. 9. Collision probability between the drone and CA with the collision and non-collision cases in Fig. 8.

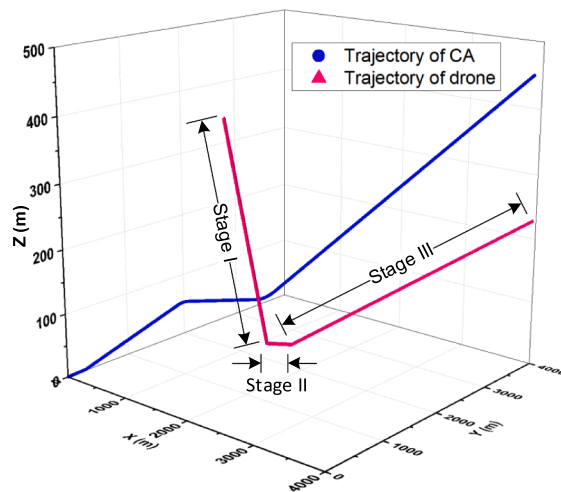


Fig. 10. Trajectories of the drone and CA with the three-stage case.

(Paielli and Erzberger, 1997). However, due to the limitation of MC simulation, the computing time increases with the number of iterations, 53.54 s with 50,000 iterations. In contrast, the computation of the proposed algorithm took only 7.93 s, which is less than the time taken by using the MC algorithm.

Reducing the computing time is critical to realize the real-time collision probability estimation so as to facilitate the on-board application. Therefore, two other simulations are conducted here to test the computational efficiency. By balancing between error accuracy and computing time from results in Table 3, MC-50,000 is served as a comparative group and the results are shown in Table 4. With the improvement of computer configuration, from Com.1 to Com.3, the computing time of the proposed method is reduced, merely 0.86 s with Com.3. Although the results of MC-50,000 show a decreasing computing time in Table 4, the fastest time 17.89 s with Com.3, still make it weaker to achieve the airborne application.

The position error of an air vehicle caused by the influence of uncertainties changes over time. Also, different uncertainties will bring about different position errors, further, corresponding to different variances and standard deviations. To test the effects of different relative position errors on the collision probability between the intruding drone and CA, sensitivity simulations are conducted. For intruding drone, DJI Mavic 2 is chosen as the intruding drone to obtain the variances in the along-track, cross-track and vertical directions. The experimental result obtained is shown in Fig. 5. Here, the drone’s initial position is set as  $X_D$  (1500, 1000, 500). The variances of CA are changing over time and their growth rates are given based on Eqs. (6)–(8),  $g_a^2 = 7.72$ ,  $g_c^2 = 13.58$  and  $g_v^2 = 8.93$ .

Given different standard deviations of the intruding drone, the results of the standard deviation of relative position error and collision probability are shown in Figs. 6 and 7. We set different values of the standard deviation of the intruding drone, specifically, zero, basic value (taken from Fig. 5), 1.5 times, and 6.0 times of basic value, respectively, to test the sensitivity of the standard deviation of relative position error. From the results shown in Fig. 6, the standard deviation of relative position error tends to increase with the growth of drone’s given standard deviation, from 0 to 6.0 times of basic value. In Fig. 7, in the case of zero position error, the

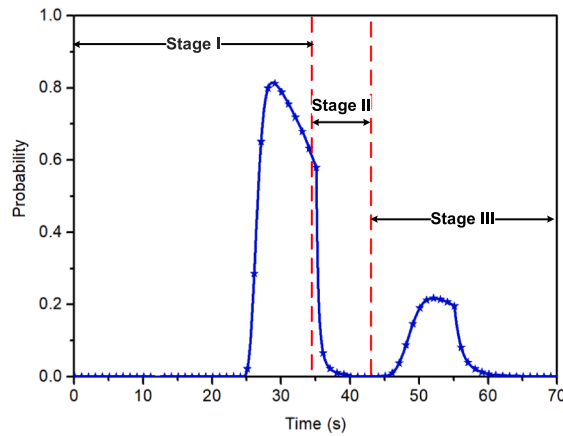


Fig. 11. Collision probability between the drone and CA with the drone’s three-stage trajectory.

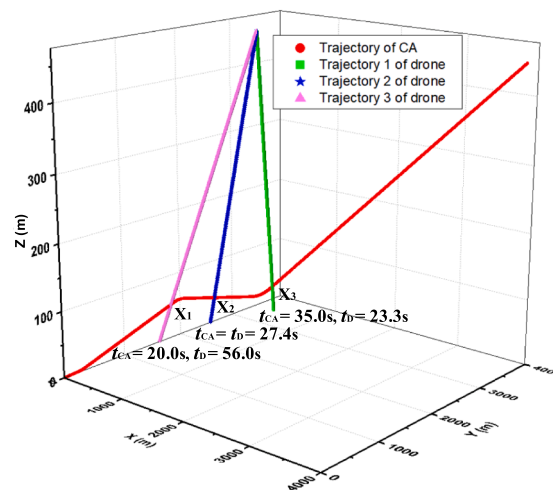


Fig. 12. Three different possible trajectories of the drone with a given trajectory of the CA.

collision probability is highest. The collision probability between the intruding drone and CA becomes lower in pace with the increase of standard deviation of relative position error. The simulation results match well with the established view that the more serious deviation caused by uncertainties leads to the greater position error of the aerial vehicles, and thus produces the lower collision probability.

#### 4.2. Collision probability simulation using given trajectories of the drone

After the computational reliability is demonstrated, by giving the trajectories of the drone, the proposed method can be applied to some special cases. For this purpose, the verification of the proposed model is completed by collision and non-collision cases, a three-phase changing trajectory case, and a different drone’s trajectories case.

For collision and non-collision cases, the initial position of the drone and CA are set as  $X_D (1353.9, 1253.9, 497.2)$  and  $X_{CA} (0, 0, 0)$ , respectively. By changing the velocity of the drone under the same initial position, the collision and non-collision trajectories are shown in Fig. 8(a) and (b). The main views and other views (small figures embedded in the main views) are given to visually observe the differences of the trajectories in two cases. Accordingly, the respective collision probability evaluation results are shown in Fig. 8. For the collision case, the collision happens at the 35th second with the minimal mean relative distance and the largest collision probability correspondingly appears at the same time in Fig. 9. For the non-collision case, the level of the collision risk is relatively lower by comparing it with the collision case. The figures covered in these two comparative cases illustrate that the smaller the distance between the drone and CA, the greater the collision probability.

Another case study is considered on the condition that the trajectory of the drone is constantly changing, a three-stage changing trajectory of the drone is simulated, as shown in Fig. 10, in which the three stages are 1st–34th, 34th–43nd and 43rd–70th, respectively. It implies that the drone over the take-off trajectory of a CA firstly approaches the CA and then turns for a short time interval

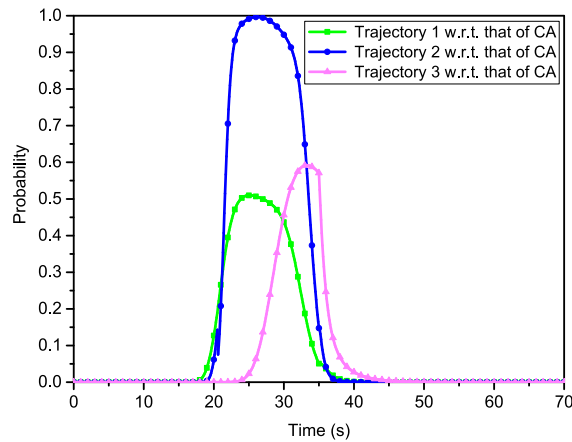


Fig. 13. Collision probability between the drone and CA with three different possible drone's trajectories.

before gradually leaving the CA. Fig. 11 shows the collision probability of the three-stage trajectory, which illustrates the trend that the smaller the relative position is, the greater the collision probability is.

In the present model, if the initial position of a drone and the trajectory of the CA are known, the probability of collision between the drone and CA can be evaluated by tracking and modeling the drone's trajectory moving to the next moment. To comparatively evaluate the collision probability of drone and CA when the drone is at the same initial position but in different trajectories, three distinct trajectories of the drone are given and simulated based on the proposed algorithm. As shown in Fig. 12, the initial position of the drone is  $X_D$  (1800, 1500, 500). As the drone flies along with Trajectory 1 and Trajectory 3, it takes the 23.3 s and 56.0 s, respectively, to arrive at the position  $X_3$  or position  $X_2$  on CA's trajectory. On the other hand, the CA takes only 35.0 s and 20.0 s, respectively, to pass these two positions. Although the drone reaches the trajectory of CA, due to the limitation of its speed and initial position, it is staggered with CA in arrival time. As a result, if the drone operates along these two trajectories, it is more likely to avoid the CA. As for the drone's trajectory 2, there exists  $t_{CA} = t_D = 27.4$  s, which means that if the drone flies according to Trajectory 2, it is projected to have a high collision probability with the CA at the position  $X_1$ . The corresponding collision probability of this case can be seen in Fig. 13, which proves that the proposed probabilistic model works well as the drone's trajectory varies.

#### 4.3. Collision probability based on collision-course trajectory planning

In this section, the cases with unknown trajectories of the drone are considered. The scheme of collision-course based trajectory planning is employed to produce the drone's trajectories on the assumption that the initial positions of the drone are known. The study cases are simulated next.

By assuming a scenario where the airport obtains the latest position information of the intruding drone after the CA takes off, the model based on the current drone's initial position can then be updated to achieve a more accurate collision probability evaluation. Fig. 14(a), (b) and (c) show the results of collision probability with the drone's positions update once and twice. Fig. 14(a) shows the once-update case where the updated position of the model tends to be far away from the trajectory of the CA. The initial position of the drone is  $X_{D1}$  (1800, 1500, 500), the update position  $X_{D2}$  (2120, 2188, 105.7) occurs at the 22.5th second. Accordingly, the collision angles change from  $(-80.8048^\circ, -80.3028^\circ)$  to  $(-82.2157^\circ, -81.8759^\circ)$ . With the same initial position, another once-update case that new update position approaches the CA's trajectory is shown in Fig. 14(b), where the update position changes into  $X_{D2}$  (1126, 1133, 101.6) and also happens at the 22.5th second. In this case, the collision angles change from  $(-80.8048^\circ, -80.3028^\circ)$  to  $(-37.1760^\circ, -30.3898^\circ)$ . It can be seen from the two once-update cases with different update positions that the updated performance of the proposed algorithm works well. For the twice-update case in Fig. 14(c), updates occur in the 22.5th and 32nd seconds and the drone's initial position and the next two updated positions are  $X_{D1}$  (800, 1500, 500),  $X_{D2}$  (2120, 2188, 105.7) and  $X_{D3}$  (2908.2, 2953.2, 248.3), respectively. In turn,  $(16.3225^\circ, 18.0423^\circ)$ ,  $(15.8162^\circ, 17.0627^\circ)$ , and  $(-76.7505^\circ, -76.1448^\circ)$  are the range of the updated collision angles. The simulation result of this case also proves that the model is still performing well with multiple updates.

The effects of the dimension of the collision zone on the collision probability will next be studied. Two cases with different radii and heights of the collision zone are simulated and the results of the collision risk evaluation are shown in Fig. 15(a) and (b), in which the initial position of the drone is set as  $X_D$  (1000, 1500, 500) and the range of the collision angle is  $(-56.8102^\circ, -52.4102^\circ)$ . When the collision height  $h = 300$  m, the collision probabilities corresponding to the 200 m, 300 m, 450 m and 600 m of the collision radii are shown in Fig. 15(a) while the collision radius  $r = 500$  m and the collision heights are 150 m, 200 m, 280 m and 400 m, respectively, the probabilities are depicted in Fig. 15(b). As can be seen from these two figures, the collision probability increases as the collision zone goes bigger.

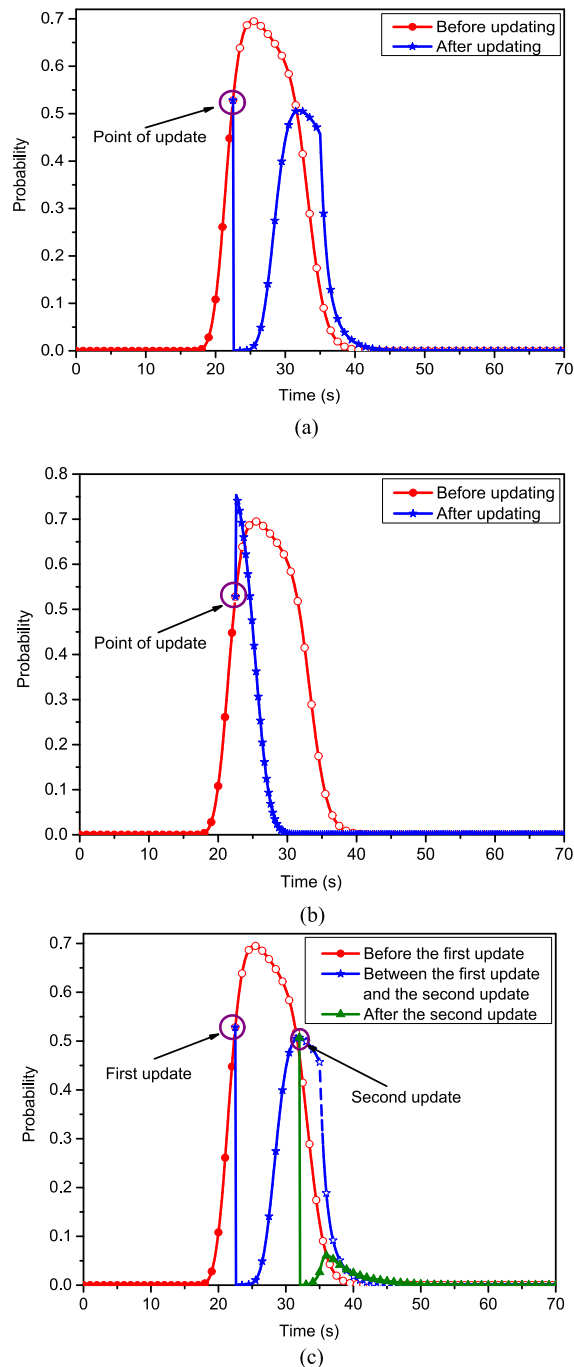
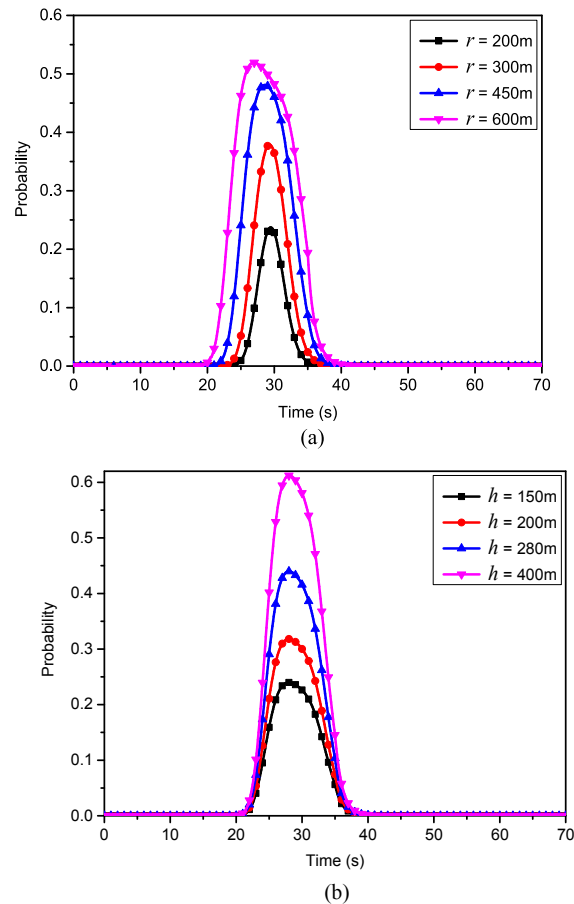


Fig. 14. Collision probability between the drone and CA for updating positions (a) one update with the “far away” trend, (b) one update with the “approach” trend, and (c) result of two-update.

### 5. Concluding remarks

The collision risk evaluation between the intruding drone and CA in the airport’s restricted area has been presented in this paper. With the assumption that the information about intruding drones near an airport is limited, the collision-course based trajectory planning of the drone is developed, given the trajectory of CA from the flight plan. The trajectories of the drone and CA are then used to provide relative position prediction. To tackle possible disturbances in the internal and/or external environment, the stochastic position prediction model based Brownian motion is introduced to evaluate the collision probability of drone operations. To demonstrate the reliability and efficiency of the proposed collision probability evaluation model, the results obtained by the method have been



**Fig. 15.** Collision probability between the drone and CA with (a) different collision radii when the collision height  $h = 300$  m and (b) different collision heights when the collision radius when the collision height  $r = 500$  m (refer to Fig. 4 for the definition of  $h$  and  $r$ ).

compared with those by MC simulations and some special cases with given trajectories of the drone, and both results match well. The paper went further to consider the collision-course based cases covering different drone's initial positions, positions update and different collision zones. The simulation results demonstrate the capability of the proposed method in evaluating the collision risk of the intruding drone and CA. The proposed approach can well adapt to the collision probability evaluation in the presence of complex and variable trajectories of the drone.

In future works, since it takes a brief time for the CA to take off from the airport restricted area or approaching safely in the restricted area of the airport (about less than 1.5 min based on the radius of 5 km around the airport, for example), it is important to assess the collision risk in the airport terminal area by constantly updating the model parameters. Also, the current work can be extended for the development of multi-drone collision risk modeling and evaluation.

#### CRedit authorship contribution statement

**Na Zhang:** Conceptualization, Investigation, Formal analysis, Methodology, Validation, Writing - original draft, Writing - review & editing. **Hu Liu:** Formal analysis, Methodology, Software, Validation, Writing - review & editing. **Bing Feng Ng:** Writing - review & editing. **Kin Huat Low:** Funding acquisition, Resources, Project administration, Methodology, Writing - review & editing, Supervision.

#### Acknowledgments

This research is supported by the Civil Aviation Authority of Singapore and the Nanyang Technological University, Singapore under their collaboration in the Air Traffic Management Research Institute. Any opinions, findings, and conclusions or recommendations expressed in this manuscript are those of the authors and do not reflect the views of the Civil Aviation Authority of Singapore.

The authors would like to thank Mr. Mingcheng Zhang for his assistance in the code development.

## Appendix A. Derivation of mean and covariance functions

Based on Eq. (15),  $\Delta\mathbf{X}(t) - \Delta\mathbf{X}(0)$  subjects to the Gaussian distribution from the properties of BM, then its mean function is

$$\mu[\Delta\mathbf{X}(t) - \Delta\mathbf{X}(0)] = \Delta\mathbf{V}_0 t \quad (\text{A.1})$$

The covariance function can be

$$\mathbf{C}[\Delta\mathbf{X}(t) - \Delta\mathbf{X}(0)] = t(\mathbf{R}_{CA,0} \mathbf{C}_{CA} \mathbf{R}_{CA,0}^T - \mathbf{R}_{D,0} \mathbf{C}_D \mathbf{R}_{D,0}^T) \quad (\text{A.2})$$

Consequently,

$$\Delta\mathbf{X}(T_1) - \Delta\mathbf{X}(0) \sim N(\Delta\mathbf{V}_0 T_1, T_1(\mathbf{R}_{CA,0} \mathbf{C}_{CA} \mathbf{R}_{CA,0}^T - \mathbf{R}_{D,0} \mathbf{C}_D \mathbf{R}_{D,0}^T)) \quad (\text{A.3})$$

Assuming that the trajectories of drone and CA are independent of each other, when the initial positions of the drone and CA yield to Gaussian distribution, the initial relative position  $\Delta\mathbf{X}(0)$  also yields to Gaussian distribution and there exists  $\Delta\mathbf{X}(0) \sim N(\Delta\mathbf{X}_0, \mathbf{C}_{CA,0} + \mathbf{C}_{D,0})$ , such that

$$\Delta\mathbf{X}(T_1) \sim N(\Delta\mathbf{X}_0 + \Delta\mathbf{V}_0 T_1, \mathbf{C}_{CA,0} + \mathbf{C}_{D,0} + T_1(\mathbf{R}_{CA,0} \mathbf{C}_{CA} \mathbf{R}_{CA,0}^T - \mathbf{R}_{D,0} \mathbf{C}_D \mathbf{R}_{D,0}^T)) \quad (\text{A.4})$$

Similarly, in the second time interval  $[T_1, T_2)$ ,

$$\Delta\mathbf{X}(T_2) - \Delta\mathbf{X}(T_1) = \Delta\mathbf{V}_1(T_2 - T_1) + \mathbf{R}_{CA,1} \mathbf{C}_{CA} [\mathbf{B}_{CA}(T_2) - \mathbf{B}_{CA}(T_1)] - \mathbf{R}_{D,1} \mathbf{C}_D [\mathbf{B}_D(T_2) - \mathbf{B}_D(T_1)] \quad (\text{A.5})$$

According to the properties of BM, the function  $\Delta\mathbf{X}(T_2) - \Delta\mathbf{X}(T_1)$  yields to Gaussian distribution such that

$$\Delta\mathbf{X}(T_2) - \Delta\mathbf{X}(T_1) \sim N(\Delta\mathbf{V}_1(T_2 - T_1), (T_2 - T_1)(\mathbf{R}_{CA,1} \mathbf{C}_{CA} \mathbf{R}_{CA,1}^T - \mathbf{R}_{D,1} \mathbf{C}_D \mathbf{R}_{D,1}^T)) \quad (\text{A.6})$$

As  $\Delta\mathbf{X}(T_2)$  subjects to Gaussian distribution, the mean and covariance functions can respectively be

$$\mu[\Delta\mathbf{X}(T_2)] = \Delta\mathbf{X}_0 + \Delta\mathbf{V}_0(T_1 - T_0) + \Delta\mathbf{V}_1(T_2 - T_1) \quad (\text{A.7})$$

$$\mathbf{C}[\Delta\mathbf{X}(T_2)] = \mathbf{C}_{CA,0} + \mathbf{C}_{D,0} + \sum_{k=0}^1 (T_{k+1} - T_k) (\mathbf{R}_{CA,k} \mathbf{C}_{CA} \mathbf{R}_{CA,k}^T + \mathbf{R}_{D,k} \mathbf{C}_D \mathbf{R}_{D,k}^T) \quad (\text{A.8})$$

which can then be deduced that the mean and covariance functions of  $\Delta\mathbf{X}(T_k)$ :

$$\mu[\Delta\mathbf{X}(T_k)] = \begin{cases} \mu[\Delta\mathbf{X}(T_0)] = \Delta\mathbf{X}_0, & k = 0 \\ \Delta\mathbf{X}_0 + \sum_{n=1}^k \Delta\mathbf{V}_{n-1}(T_n - T_{n-1}), & 0 < k \leq N \end{cases} \quad (\text{A.9})$$

$$\mathbf{C}[\Delta\mathbf{X}(T_k)] = \begin{cases} \mathbf{C}_{CA,0} + \mathbf{C}_{D,0}, & k = 0 \\ \mathbf{C}_{CA,0} + \mathbf{C}_{D,0} + \sum_{n=1}^k (T_n - T_{n-1}) (\mathbf{R}_{CA,n-1} \mathbf{C}_{CA} \mathbf{R}_{CA,n-1}^T + \mathbf{R}_{D,n-1} \mathbf{C}_D \mathbf{R}_{D,n-1}^T), & 0 < k \leq N \end{cases} \quad (\text{A.10})$$

$$\mu[\Delta\mathbf{X}(t)] = \mu[\Delta\mathbf{X}(T_k)] + \Delta\mathbf{V}_k(t - T_k) \quad (\text{A.11})$$

$$\mathbf{C}[\Delta\mathbf{X}(t)] = \mathbf{C}[\Delta\mathbf{X}(T_k)] + (t - T_k) (\mathbf{R}_{CA,k} \mathbf{C}_{CA} \mathbf{R}_{CA,k}^T - \mathbf{R}_{D,k} \mathbf{C}_D \mathbf{R}_{D,k}^T) \quad (\text{A.12})$$

## Appendix B. Coordinate transformation

In Fig. B.1, the circle with  $O_c$  as its center and  $r$  as its radius is the horizontal projection of the collision zone and the ellipse with  $O_{e'}$  as its center represents the error ellipse in the horizontal projection of the relative position of the two aerial vehicles. Let the point  $O_{e'}(0, 0)$  in the coordinate system  $x_t' O_{e'} y_t'$  be  $O_{e'}(\mu_{x_t}, \mu_{y_t})$  in the coordinate system  $x_t O_c y_t$ , and the angle between the direction of the long axis of the error ellipse and the  $x_t$  axis be

$$\varphi_t = \arccos \frac{\Delta\mathbf{V}_t \mathbf{n}}{|\Delta\mathbf{V}_t| |\mathbf{n}|} \quad (\mathbf{n} = (0, 0, 1)^T) \quad \text{and } 0 \leq \varphi_t \leq \pi \quad (\text{B.1})$$

and there exists a rotation matrix

$$\mathbf{R}(\varphi_{T_k}) = \begin{pmatrix} \cos\varphi_{T_k} & -\sin\varphi_{T_k} \\ \sin\varphi_{T_k} & \cos\varphi_{T_k} \end{pmatrix} \quad (\text{B.2})$$

(also denoted as  $\mathbf{R}_{T_k}$ ), such that point  $(x_t, y_t)$  in the coordinate system  $x_t O_c y_t$  can be

$$\begin{pmatrix} x_t' \\ y_t' \end{pmatrix} = \mathbf{R}_{T_k} \begin{pmatrix} x_t - \mu_{x_t} \\ y_t - \mu_{y_t} \end{pmatrix} \tag{B.3}$$

in the coordinate system  $x_t' O_{e_t} y_t'$ . Thus, the collision circle center  $O_{c_t}(0, 0)$  in the coordinate system  $x_t O_{c_t} y_t$  will be

$$\begin{pmatrix} a_t \\ b_t \end{pmatrix} = \mathbf{R}_{T_k} \begin{pmatrix} -\mu_{x_t} \\ -\mu_{y_t} \end{pmatrix} \tag{B.4}$$

in the coordinate system  $x_t' O_{e_t} y_t'$ , and the equation of collision circle can be

$$(x_t' - a_t)^2 + (y_t' - b_t)^2 = r^2 \tag{B.5}$$

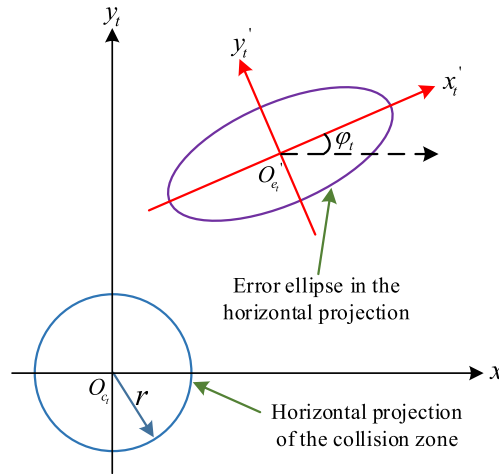


Fig. B1. Coordinate transformation for error ellipse.

### Appendix C. Supplementary material

Supplementary data to this article can be found online at <https://doi.org/10.1016/j.trc.2020.102736>.

### References

Airbus, S., 2005. Aircraft characteristics airport and maintenance planning. Blagnac.

Ali, B.S., 2016. System specifications for developing an Automatic Dependent Surveillance-Broadcast (ADS-B) monitoring system. *Int. J. Crit. Infrastruct. Prot.* 15, 40–46.

Arblaster, M., 2018. New Entrants Into Airspace—Unmanned Aircraft (“Drones”) and Increased Space Transportation. In: Arblaster, M. (Ed.), *Air Traffic Management*. Elsevier.

Bai, H., Hsu, D., Kochenderfer, M. J., Lee, W. S., 2012. Unmanned aircraft collision avoidance using continuous-state POMDPs. *Robot. Sci. Syst.* VII 1, 1–8.

Balakrishnan, H., 2016. Control and optimization algorithms for air transportation systems. *Ann. Rev. Control* 41, 39–46.

Barlow, Z., Jashami, H., Sova, A., Hurwitz, D.S., Olsen, M.J., 2019. Policy processes and recommendations for Unmanned Aerial System operations near roadways based on visual attention of drivers. *Transp. Res. Part C: Emerg. Technol.* 108, 207–222.

Chryssanthacopoulos, J.P., Kochenderfer, M.J., 2011. Accounting for state uncertainty in collision avoidance. *J. Guid. Control Dyn.* 34, 951–960.

Deulgaonkar, P., 2017. Shutting down dubai international airport due to a drone costs \$100000 a minute. *Arabian Business*, <https://www.arabianbusiness.com/content/375851-drone-costs-100000-minute-loss-to-uae-airports> (accessed 5 May 2020).

DJI Technology Co., L., 2019. Mavic 2 - Specifications, FAQs, Videos, Tutorials, Manuals - DJI. SZ DJI Technology Co, Ltd, Shenzhen, China.

Dogan, A., Zengin, U., 2006. Unmanned aerial vehicle dynamic-target pursuit by using probabilistic threat exposure map. *J. Guid. Control Dyn.* 29, 944–954.

Driessen, S.P.H., Janssen, N.H.J., Wang, L., Palmer, J.L., Nijmeijer, H., 2018. Experimentally Validated Extended Kalman Filter for UAV State Estimation Using Low-Cost Sensors. *IFAC-PapersOnLine* 51, 43–48.

Du, W.B., Zhang, M.Y., Zhang, Y., Cao, X.B., Zhang, J., 2018. Delay causality network in air transport systems. *Transp. Res. Part E: Log. Transp. Rev.* 118, 466–476.

Glover, W., Lygeros, J., 2004. A multi-aircraft model for conflict detection and resolution algorithm evaluation. *HYBRIDGE Deliv. D* 1, 3.

Hu, J., Lygeros, J., Prandini, M., Sastry, S., 1999. Aircraft conflict prediction and resolution using Brownian Motion. In: *Proceedings of the 38th IEEE Conference on Decision and Control* (Cat. No. 99CH36304). IEEE, pp. 2438–2443.

Kacem, T., Barreto, A., Wijesekera, D., Costa, P., 2017. ADS-Bsec: A novel framework to secure ADS-B. *ICT Express* 3, 160–163.

La Cour-Harbo, A., Schjoler, H., 2019. Probability of low altitude midair collision between general aviation and unmanned aircraft. *Risk Anal.* 39 (11), 2499–2513.

Lascara, B.J., Carson, J.W., Edwards, D.N., 2013. A study of primary surveillance radar traffic and its utility via ADS-B uplink. In: *2013 Integrated Communications, Navigation and Surveillance Conference (ICNS)*. IEEE, pp. 1–11.

Li, D., Cui, D., 2008. Air traffic control conflict detection algorithm based on Brownian motion. *J.-Tsinghua Univ.* 48, 477.

- Liu, H., Mohd, H.C.M., Ng, B.F., Low, K.H., 2020. Airborne Collision Evaluation between Drone and Aircraft Engine: Effects of Position and Posture on Damage of Fan Blades. In: AIAA Aviation 2020 Forum. <https://doi.org/10.2514/6.2020-3214>.
- Luo, C., McClean, S.I., Parr, G., Teacy, L., De Nardi, R., 2013. UAV position estimation and collision avoidance using the extended Kalman filter. *IEEE Trans. Veh. Technol.* 62, 2749–2762.
- Maracich, F., 2006. Flying free flight: pilot perspective and system integration requirement. *IEEE Aerosp. Electron. Syst. Mag.* 21, 3–7.
- Matsuno, Y., Tsuchiya, T., Wei, J., Hwang, I., Matayoshi, N., 2015. Stochastic optimal control for aircraft conflict resolution under wind uncertainty. *Aerosp. Sci. Technol.* 43, 77–88.
- Michalski, D., Michalska, A., 2017. Protection against drone activity. In: Security Forum. Wydawnictwo Naukowe Akademii WSB, pp. 73–83.
- Munoz, C., Narkawicz, A., Chamberlain, J., 2013. A TCAS-II resolution advisory detection algorithm. In: AIAA Guidance, Navigation, and Control (GNC) Conference, p. 4622.
- Netjasov, F., Crnogorac, D., Pavlović, G., 2019. Potential safety occurrences as indicators of air traffic management safety performance: A network based simulation model. *Transp. Res. Part C: Emerg. Technol.* 102, 490–508.
- Paielli, R.A., Erzberger, H., 1997. Conflict probability estimation for free flight. *J. Guid. Control Dyn.* 20, 588–596.
- Paielli, R.A., Erzberger, H., 1999. Conflict probability estimation generalized to non-level flight. *Air Traffic Control Quart.* 7, 195–222.
- Peng, T., Su, L., Zhang, R., Guan, Z., Zhao, H., Qiu, Z., Zong, C., Xu, H., 2020. A new safe lane-change trajectory model and collision avoidance control method for automatic driving vehicles. *Exp. Syst. Appl.* 141 <https://doi.org/10.1016/j.eswa.2019.112953>.
- Prandini, M., Hu, J., Lygeros, J., Sastry, S., 2000. A probabilistic approach to aircraft conflict detection. *IEEE Trans. Intell. Transp. Syst.* 1, 199–220.
- Prandini, M., Lygeros, J., Nilim, A., Sastry, S., 1999. Randomized algorithms for probabilistic aircraft conflict detection. In: Proceedings of the 38th IEEE Conference on Decision and Control (Cat. No. 99CH36304). IEEE, pp. 2444–2449.
- Prandini, M., Watkins, O.J., 2005. Probabilistic aircraft conflict detection. HYBRIDGE, IST-2001 32460.
- Prevost, C.G., Desbiens, A., Gagnon, E., 2007. Extended Kalman filter for state estimation and trajectory prediction of a moving object detected by an unmanned aerial vehicle. In: 2007 American control conference. IEEE, pp. 1805–1810.
- Qiming, Y., Jiandong, Z., Guoqing, S., 2019. Modeling of UAV path planning based on IMM under POMDP framework. *J. Syst. Eng. Electron.* 30, 545–554.
- Radanovic, M., Pjera Eroles, M.A., Koca, T., Ramos Gonzalez, J.J., 2018. Surrounding traffic complexity analysis for efficient and stable conflict resolution. *Transp. Res. Part C: Emerg. Technol.* 95, 105–124.
- Riahi Manesh, M., Kaabouch, N., 2017. Analysis of vulnerabilities, attacks, countermeasures and overall risk of the Automatic Dependent Surveillance-Broadcast (ADS-B) system. *Int. J. Crit. Infrastruct. Prot.* 19, 16–31.
- Romli, F., King, J., Li, L., Clarke, J.P., 2008. Impact of automatic dependent surveillance-broadcast (ADS-B) on traffic alert and collision avoidance system (TCAS) performance. In: AIAA Guidance, Navigation and Control Conference and Exhibit. <https://doi.org/10.2514/6.2008-6971>.
- Roudet, J., Thurat, P.E., Turcot, N., 2016. Airport Ground-traffic Surveillance Systems Data Feed Innovative Comprehensive Analysis. *Transp. Res. Procedia* 14, 3741–3750.
- Schaufele, R., Ding, L., Miller, N., Barlett, H., Lukacs, M., Bhadra, D., 2017. FAA aerospace forecast: Fiscal years 2017–2037. United States Department of Transportation, Washington, DC.
- Schlag, C., 2012. New Privacy Battle: How the Expanding Use of Drones Continues to Erode Our Concept of Privacy and Privacy Rights. *The Pitt. J Tech L & Pol'y* 13.
- Shi, L., Wu, R., 2012. A probabilistic conflict detection algorithm in terminal area based on three-dimensional Brownian motion. In: 2012 IEEE 11th International Conference on Signal Processing. IEEE, pp. 2287–2291.
- Shi, X., Yang, C., Xie, W., Liang, C., Shi, Z., Chen, J., 2018. Anti-drone system with multiple surveillance technologies: Architecture, implementation, and challenges. *IEEE Commun. Mag.* 56, 68–74.
- Stubberud, S.C., Kramer, K.A., 2007. Predictive guidance intercept using the neural extended Kalman filter tracker. *Control Intell. Syst.* 35, 228–235.
- Sturdivant, R.L., Chong, E.K., 2017. Systems engineering baseline concept of a multispectral drone detection solution for airports. *IEEE Access* 5, 7123–7138.
- Sun, J., Blom, H.A.P., Ellerbroek, J., Hoekstra, J.M., 2019a. Particle filter for aircraft mass estimation and uncertainty modeling. *Transp. Res. Part C: Emerg. Technol.* 105, 145–162.
- Sun, J., Ellerbroek, J., Hoekstra, J.M., 2019b. WRAP: An open-source kinematic aircraft performance model. *Transp. Res. Part C: Emerg. Technol.* 98, 118–138.
- Tang, J., 2017. Analysis and Improvement of Traffic Alert and Collision Avoidance System. *IEEE Access* 5, 21419–21429.
- Tang, J., Pjera, M.A., Guasch, T., 2016. Coloured Petri net-based traffic collision avoidance system encounter model for the analysis of potential induced collisions. *Transp. Res. Part C: Emerg. Technol.* 67, 357–377.
- Tang, J., Zhu, F., Pjera, M.A., 2018. A causal encounter model of traffic collision avoidance system operations for safety assessment and advisory optimization in high-density airspace. *Transp. Res. Part C: Emerg. Technol.* 96, 347–365.
- Teixeira, B.O., Torres, L.A., Iscolod, P., Aguirre, L.A., 2011. Flight path reconstruction—A comparison of nonlinear Kalman filter and smoother algorithms. *Aerosp. Sci. Technol.* 15, 60–71.
- Wang, C.H.J., Tan, S.K., Low, K.H., 2019a. Collision Risk Assessment between UAS and Landing Aircraft in Restricted Airspace Surrounding an Airport using 3D Monte-Carlo Simulation. In: AIAA Aviation 2019 Forum. <https://doi.org/10.2514/6.2019-3185>.
- Wang, C.J., Tan, S.K., Low, K.H., 2019b. Collision risk management for non-cooperative UAS traffic in airport-restricted airspace with alert zones based on probabilistic conflict map. *Transp. Res. Part C: Emerg. Technol.* 109, 19–39.
- Wang, C.J., Tan, S.K., Low, K.H., 2020. Three-dimensional (3D) Monte-Carlo modeling for UAS collision risk management in restricted airport airspace. *Aerosp. Sci. Technol.* 105, 105964.
- Zhang, X., Zhang, J., Wu, S., Cheng, Q., Zhu, R., 2018. Aircraft monitoring by the fusion of satellite and ground ADS-B data. *Acta Astronaut.* 143, 398–405.
- Zhu, Y., Wang, J., Chen, Y., Wu, Y., 2016. Calculation of Takeoff and Landing Performance under Different Environments. In: International Journal of Modern Physics: Conference Series. World Scientific. <https://doi.org/10.1142/S2010194516601745>.